Letter Vol. 5, No. 11 / November 2018 / Optica 1414

optica

Characterizing optical resonances using spatial mode reshaping

Wei Zhang,[1,*] Aaron Charous,[1] Masaya Nagai,[2] Daniel M. Mittleman,[1] and Rajind Mendis[1]

[1]School of Engineering, Brown University, Providence, Rhode Island 02912, USA
[2]Graduate School of Engineering Science, Osaka University, Toyonaka, Osaka 560-8531, Japan
*Corresponding author: wei_zhang@brown.edu

Received 10 July 2018; revised 18 October 2018; accepted 19 October 2018 (Doc. ID 338334); published 2 November 2018

Accurately characterizing the width of a narrow (high Q) resonance can be quite challenging, requiring either a high-resolution grating spectrometer or a Fourier transform spectrometer with a long delay range. Here, we describe a new technique to determine the Q of a resonance based on spatial measurements that is not subject to the same limitations as conventional methods. We theoretically show that this technique can give an accurate measurement of Q for essentially any set of input beam parameters, even if the spectral resolution of the measurement is inadequate to resolve the linewidth of the resonance. We confirm this striking result with both numerical simulations and experimental measurements.

https://doi.org/10.1364/OPTICA.5.001414

Planar optical systems, ranging from the simplest total internal reflection system to more complicated systems such as gratings, surface plasmonic systems, metasurfaces, artificial-dielectric slabs, and photonic crystal slabs, are important in many areas of optics [1]. For many years, researchers have studied the change in the spatial distribution of a beam, which can be induced by interactions with planar systems. The most relevant of these involves the Goos–Hänchen effect, a phenomenon in which a light beam exhibits a lateral shift in its centroid position upon total internal reflection from an interface [2,3]. This effect originates from the fact that different angular components in a beam acquire different phases upon reflection. The magnitude of the lateral shift is given by the slope of the phase change, $-\partial\varphi/\partial k_{\|}$, where φ is the phase of the complex reflection coefficient and $k_{\|} = k \sin\theta$ is the parallel momentum (PM) of the incident radiation (i.e., the projected k-vector parallel to the interface) [3,4]. Similar effects have also been observed in systems that exhibit resonances [5–7] caused by the dramatic phase change near the resonant conditions. Unlike the simpler case of total internal reflection, these examples can exhibit a more complicated amplitude and phase response, particularly when the linewidth of the resonance is small. The lateral shift is often accompanied by expansions and distortions of the beam profile [8,9]. In some cases, an incident Gaussian beam profile can split into two distinct lobes with comparable amplitudes after interacting with a resonant system [10–12]. Although this complex behavior has been observed previously, the analysis has never included any consideration beyond that of a simple Goos–Hänchen shift, which is unable to account for splitting or distortions of the beam shape.

Here, we develop a general formalism to describe these spatial distortions. We find that, for some specific conditions, the output beam profile is almost identical to the incident beam profile, but laterally shifted, corresponding to the familiar Goos–Hänchen effect. However, in other cases, the beam profile changes significantly, such that the Goos–Hänchen description is no longer valid. Nevertheless, we find in all cases that the spatial mode contains a signature of the linewidth of the resonance, which can be exploited for spectroscopic purposes. Conventionally, accurately characterizing the width of a narrow (high Q) resonance can be quite challenging, requiring either a high-resolution grating spectrometer or a Fourier transform spectrometer with a long delay range [13]. The proposed new technique based on the spatial measurements, however, is not subject to the same limitations as the conventional spectral methods. We show that this technique can give an accurate measurement of Q for essentially any set of input beam parameters, even if the spectral resolution of the measurement is inadequate to resolve the linewidth of the resonance. Moreover, this technique converges in the presence of noise more rapidly than a high-resolution spectroscopic measurement. We experimentally verify the validity of our method using an artificial-dielectric structure that exhibits bound states in the continuum (BIC) resonances [14] in the terahertz range [15].

We consider the optical response of a general planar system, which depends on both the incident angle (θ) and the frequency (f) of the incident radiation. Figure 1 shows a typical narrow optical resonance (green region in Fig. 1) from a planar system on the $f - k_{\|}$ diagram. One could obtain the frequency spectrum of this resonance by fixing the incident angle and scanning the frequency, which is equivalent to scanning along a tilted straight line $f = k_{\|}c/(2\pi \sin\theta)$ on the $f - k_{\|}$ diagram (red line in Fig. 1). Alternatively, one could obtain the PM spectrum of the same resonance by fixing the frequency and scanning the incident angle, which is equivalent to scanning along a horizontal line on this diagram (blue line in Fig. 1). If the resonance is not parallel to either the frequency-spectrum line or the PM-spectrum

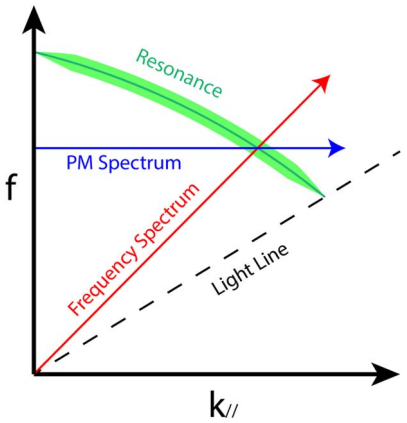

Fig. 1. $f - k_{\|}$ diagram of an optical resonance from a planar system. The resonance (green line) can be measured on a frequency spectrum with a fixed incident angle (along the red line) or on a PM spectrum with a fixed frequency (along the blue line). The linewidths from the two methods are linearly related as $\delta_f = \rho \cdot \delta_{PM}$ for narrow resonances.

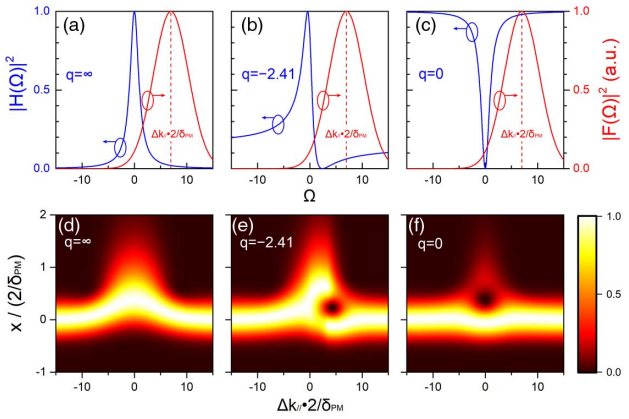

Fig. 2. Examples of spatial reshaping from Fano resonances. (a)–(c) Blue curves illustrate the spectra of Fano resonances with $q = \infty$, −2.41, and 0 as functions of dimensionless PM spectra (Ω). Red curves illustrate the PM spectra of the incident Gaussian beam $|F(\Omega)|^2$ whose spectral center is offset from the resonance by $\Delta k_{\|}$ (or $\Delta k_{\|} \cdot 2/\delta_{PM}$ for the dimensionless PM offset). (d)–(f) Normalized spatial intensity profile of the output beam as a function of the dimensionless PM offset $\Delta k_{\|} \cdot 2/\delta_{PM}$ when the input Gaussian beam interacts with the Fano resonances with $q = \infty$, −2.41, and 0. Spatial reshaping of the beam profile near the resonant condition ($\Delta k_{\|} \cdot 2/\delta_{PM} = 0$) can be clearly observed.

line (as in the case illustrated in Fig. 1, and which is true for many planar optical systems [14–16]), a resonant response would be observed in both cases with full widths at half maxima (FWHMs) of δ_f and δ_{PM}, respectively. For narrow resonances, δ_f and δ_{PM} are linearly related as

$$\delta_f = \rho \cdot \delta_{PM}, \tag{1}$$

where the ratio ρ is determined by the incident angle and the rate of change of the resonant frequency versus incident angle (see Supplement 1).

As a generalized version of a Lorentzian lineshape, a Fano lineshape is widely used to describe resonances in many optical systems, including plasmonic nanostructures, metamaterials, photonic crystals, and other types of optical cavities [17–22]. It is also the only possible lineshape for certain types of resonators [19]. To characterize a general resonance in a planar optical system, we assume a Fano lineshape with an intensity spectrum described by [23]

$$|H(\Omega)|^2 = D^2 \frac{(q + \Omega)^2}{1 + \Omega^2}. \tag{2}$$

Here, we express the resonance not as a function of frequency (as is more common), but rather as a function of the PM to capture the notion that this resonance can be characterized in either of the two ways shown in Fig. 1. The dimensionless PM parameter Ω is given by $\Omega = \pm 2(k_{\|} - k_{\|0})/\delta_{PM}$ [i.e., the PM offset from the resonant condition ($k_{\|} = k_{\|0}$) normalized by half the FWHM, where the sign depends on the choice of positive direction]. Without a loss of generality, we let $\Omega = 2(k_{\|} - k_{\|0})/\delta_{PM}$. In Eq. (2), q is the usual Fano resonance parameter (which could be a complex number, corresponding to the case of incomplete extinction [22]) and D is a normalization constant. The blue curves in Figs. 2(a)–2(c) illustrate the intensity spectrum $|H(\Omega)|^2$ as a function of Ω for a few particular choices of q. The complex amplitude spectrum has the form [22,24],

$$H(\Omega) = \frac{1}{2}\left(e^{-2i\operatorname{arccot}(q)} + \frac{1 - i\Omega}{1 + i\Omega}\right). \tag{3}$$

As a result, the impulse response (or Green's function) of this optical system is (see Supplement 1)

$$h(x) = -\frac{1}{1 - iq}\delta(x) + \frac{\delta_{PM}}{2}u(x)e^{ik_{\|0}x}e^{-x\delta_{PM}/2}, \tag{4}$$

where x is the spatial displacement along the surface of the planar optical system, $\delta(x)$ is the Dirac delta function, and $u(x)$ is the Heaviside step function. Equation (4) indicates that, with a given incident amplitude profile $f(x)$, the output amplitude profile $g(x) = h(x) * f(x)$ is the superposition of the (scaled) incident spatial profile [the first term of Eq. (4)] and a spatially more extended term [the second term of Eq. (4)].

Specifically, we consider an incident beam with a Gaussian profile. We assume that this beam has a complex amplitude profile $f(x) = \exp[i(k_{\|0} + \Delta k_{\|})x - x^2/(2w_0^2)]$ at the surface of the planar optical system, where $\Delta k_{\|}$ is the PM offset from the resonant condition (defined by $k_{\|} = k_{\|0}$, or $\Omega = 0$) and w_0 is the radius of the Gaussian beam. By substituting this expression for $f(x)$ and using Eq. (4), we obtain the spatial intensity profile of the output beam (along the surface),

$$|g(x)|^2 = \left| -\frac{1}{1 - iq}f(x) + e^{ik_{\|0}x}v(x)e^{-x\delta_{PM}/2}\right|^2, \tag{5}$$

where

$$v(x) = \sqrt{\frac{\pi}{2}}\frac{\delta_{PM}}{2}w_0 e^{\frac{w_0^2}{2}\left(\frac{\delta_{PM}}{2} + i\Delta k_{\|}\right)^2} \cdot \operatorname{erfc}\left[\frac{w_0}{\sqrt{2}}\left(\frac{\delta_{PM}}{2} + i\Delta k_{\|}\right) - \frac{x}{\sqrt{2}w_0}\right] \tag{6}$$

is the decay amplitude.

This result encompasses both the familiar Goos–Hänchen effect and more complicated situations. When the incident PM spectrum is narrow ($w_0\delta_{PM} \gg 1$) or not too broad but centered far from the resonant condition ($w_0\delta_{PM} \sim 1$ and $|\Delta k_{\|}| \gg \delta_{PM}$), and is centered where the amplitude response of the system is far from zero ($|H(\Omega)| \neq 0$ when Ω is close to $2\Delta k_{\|}/\delta_{PM}$), Eq. (5) can be approximated as (see Supplement 1)

$$|g(x)|^2 \approx C \cdot |f(x-\Delta x)|^2, \tag{7}$$

for $|x| < w_0$ or $|x| \sim w_0$ (near the beam center), where

$$C = \frac{(2\Delta k_{\parallel} + \delta_{\mathrm{PM}} q)^2}{(1+q^2)(4\Delta k_{\parallel}^2 + \delta_{\mathrm{PM}}^2)} \exp\left(\frac{\Delta x^2}{w_0^2}\right), \tag{8}$$

and

$$\Delta x = \frac{2\delta_{\mathrm{PM}}}{4\Delta k_{\parallel}^2 + \delta_{\mathrm{PM}}^2}. \tag{9}$$

Equation (7) indicates that, under the above conditions, the output intensity profile is approximately identical to the incident profile (scaled by a factor of C) near the beam center, but laterally shifted by Δx, corresponding to the Goos–Hänchen effect. However, when these conditions are not met, the output beam has a complicated profile. For example, Figs. 2(d)–2(f) illustrate the normalized output intensity profiles as a function of the dimensionless incident PM offset $2\Delta k_{\parallel}/\delta_{\mathrm{PM}}$, calculated from Eq. (5) using $w_0\delta_{\mathrm{PM}} = 0.6$. As expected, we observe a simple lateral shift of the output beam profile away from the resonant condition, but complicated behaviors, including expansions and distortions, and even the splitting of the beam into two distinct lobes in Figs. 2(e) and 2(f), near the resonant condition.

Despite this large range of complicated possibilities, Eqs. (5) and (6) nevertheless exhibit a surprising and useful general feature. When the spatial coordinate is much larger than the radius of the incident Gaussian beam ($x \gg w_0$), the intensity profile $|g(x)|^2$ always decays exponentially as $\exp(-x\delta_{\mathrm{PM}})$. This result is independent of the resonator and incident beam parameters (even if the beam is off-resonance or has a PM spectrum broader than the resonance). The incident beam profile is not restricted to a Gaussian shape: As long as the incident intensity profile decays with a rate faster than $\exp(-x\delta_{\mathrm{PM}})$, the output profile always decays as $\exp(-x\delta_{\mathrm{PM}})$ for large x. Thus, we can obtain the PM-domain FWHM of a resonance from the spatial decay of the transmitted or reflected mode. Strikingly, this approach can be used to determine the intrinsic linewidth of a resonance without any requirement on the frequency or angular resolution of the measurement, because both the on- and off-resonant components of the incident beam lead to spatially decaying output profiles with the same decay rate (although the amplitude is different). We can also show that the method is more robust against measurement noise than traditional spectroscopic methods (see Supplement 1).

We now discuss a specific illustrative example, using a BIC resonance [14]. Near such a resonance, slightly tuning the geometrical parameters leads to dramatic changes in the resonance linewidth. We have recently shown that a periodic array of thin (lossless) metal plates [Fig. 3(a)] can support BICs for particular structural parameters [15]. We calculate the transmission spectrum of such a structure for p-polarized incident plane waves using the modal expansion method [25] and extract the FWHM of one of the resonances (see Supplement 1) as a function of the plate separation d. At $d \approx 1.12$ mm, the linewidth of the resonance vanishes, corresponding to a BIC. We then perform finite element method (FEM) simulations [Fig. 3(b)] and determine the linewidth from these simulations using the spatial-decay method. These values agree with the results from the rigorous calculation [Fig. 3(d)]. We note that a spectroscopic measurement with the same incident beam cannot resolve the intrinsic linewidth of the resonance when it is below ~1 GHz [dashed line in Fig. 3(d)], due to the limited PM resolution.

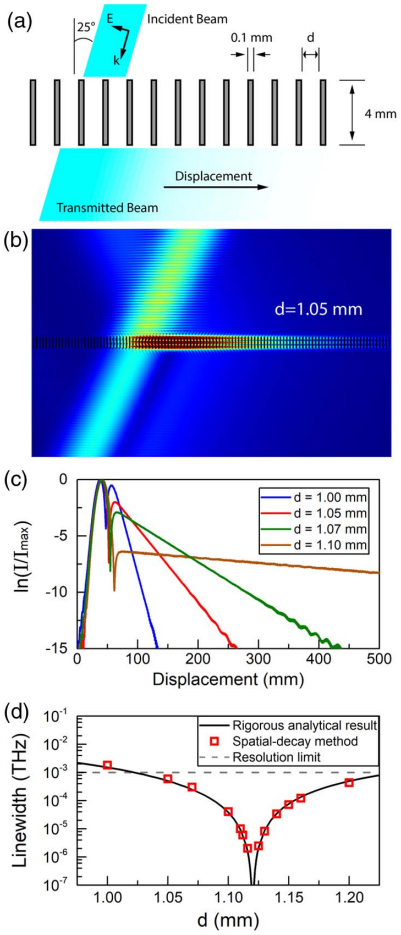

Fig. 3. FEM simulations of a specific resonant structure: a uniform array of thin metal plates. (a) An incident Gaussian beam illuminates an array of thin (lossless) metal plates with plate widths of 4 mm, plate thicknesses of 0.1 mm, plate separations of d, and an incident angle of 25°. The transmitted beam profile has spatial reshaping due to interaction with the resonance of the structure. (b) FEM simulation of the transmission near the resonance of the structure ($d = 1.05$ mm). (c) Logarithm of the simulated transmitted beam intensities as functions of displacement for various values of d. For large displacement, linear relationships can be clearly observed. Their slopes can be used to extract the linewidth of the resonance. (d) FWHM of the resonance as a function of d extracted from the simulations via the spatial-decay method (red squares), which match the rigorous analytical result (black curve). The dashed horizontal line shows the approximate limit of the linewidth that could be resolved using conventional spectroscopic methods, using the assumed PM resolution for the input beam.

In addition to this numerical analysis, we also perform experiments on a similar structure (see Supplement 1). We fabricate a device as in Fig. 3(a) with $d = 1$ mm, using a set of thin titanium plates, fabricated by chemical etching and stacked with precision spacers to form a uniformly spaced array. This is similar to the devices described in [15,26]. We measure the intensity profile of the transmitted beam at various frequencies, using terahertz time-domain spectroscopy [27]. With the highest spectral resolution available (i.e., the longest scan in the time domain), we determine that the intrinsic linewidth of the resonance is 3.31 GHz. Far from the resonance [red dots in Figs. 4(a) and 4(b)],

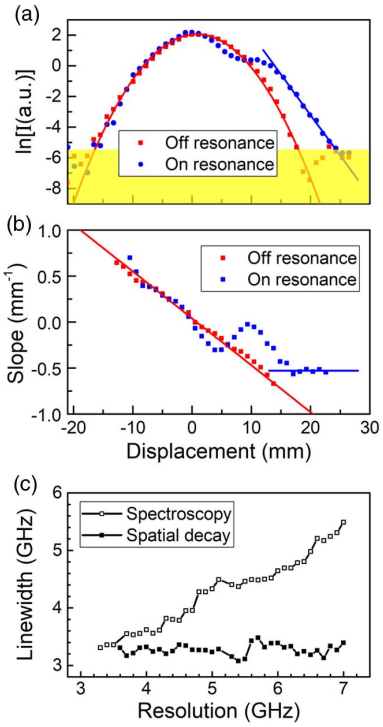

Fig. 4. Experimental results on a specific resonant structure: a uniform array of thin metal plates. (a) Experimental transmitted beam intensities as functions of displacement at 177.4 GHz (on resonance, blue dots) and at 146.6 GHz (off resonance, red dots). (b) Slopes of the profiles in (a) as a function of displacement. Off resonance (red dots), the slope changes linearly with the displacement (fitted as the red line), indicating a Gaussian spatial profile. On resonance (blue dots), a plateau is observed for large displacement (fitted as the blue line), indicating an exponential decay in the spatial profile. (c) Experimental FWHM of the same resonance from the spatial-decay method (solid dots) and the traditional spectroscopic method (empty dots) as functions of experimental frequency resolution. The spatial-decay method can accurately determine the intrinsic linewidth of the resonance, even if the linewidth is smaller than the frequency resolution.

the logarithm of the intensity profile shows a quadratic dependence, and its slope shows a linear dependence, indicating a Gaussian output profile. On resonance [blue dots in Figs. 4(a) and 4(b)], the logarithm of the intensity profile shows a linear dependence for large displacement, and the slope plateaus for large displacement, which is exactly as predicted. Using this slope at large displacement, we find a linewidth of 3.3 GHz, in excellent agreement with the value obtained using the conventional method.

Using the same experimental data, we can artificially degrade the measurement's spectral resolution by manually truncating the time-domain waveforms prior to Fourier transform. This allows us to simulate the dependence of our results on the measurement resolution. From these truncated waveforms, we find that the measured linewidth from the traditional spectroscopic method increases in direct proportion to the spectral resolution [open symbols in Fig. 4(c)], as one would expect for a resolution-limited result. However, even with degraded spectral resolution, the linewidth obtained from the spatial decay method remains approximately constant [solid symbols in Fig. 4(c)]. Remarkably, even with a time-domain waveform truncated to only 143 ps (corresponding to a spectral resolution of 7 GHz), we can still obtain a reasonably accurate measurement of the 3.3 GHz linewidth.

In conclusion, we have derived a general expression for the complicated spatial mode of an incident beam interacting with a Fano resonance, as a generalization of the well-known Goos–Hänchen effect. We find a general property of the output spatial profiles, which offers what we believe is a new method to characterize optical resonances. This method allows us to determine the intrinsic linewidth of a resonance even if the frequency or angular resolution of the incident beam is insufficient to do so, and therefore could have important applications in the characterization of narrow optical resonances.

Funding. National Science Foundation (NSF) (1609521).

See Supplement 1 for supporting content.

REFERENCES

1. P. Genevet, F. Capasso, F. Aieta, M. Khorasaninejad, and R. Devlin, Optica **4**, 139 (2017).
2. F. Goos and H. Hänchen, Ann. Phys. **436**, 333 (1947).
3. K. Y. Bliokh and A. Aiello, J. Opt. **15**, 014001 (2013).
4. K. Artmann, Ann. Phys. **437**, 87 (1948).
5. L.-G. Wang and S.-Y. Zhu, Opt. Lett. **31**, 101 (2006).
6. J. Hao, H. Li, C. Yin, and Z. Cao, J. Opt. Soc. Am. B **27**, 1305 (2010).
7. P. Ma and L. Gao, Opt. Express **25**, 9676 (2017).
8. Y. Wan, Z. Zheng, W. Kong, X. Zhao, and J. Liu, IEEE Photon. J. **5**, 7200107 (2013).
9. Y. Fan, N.-H. Shen, F. Zhang, Z. Wei, H. Li, Q. Zhao, Q. Fu, P. Zhang, T. Koschny, and C. M. Soukoulis, Adv. Opt. Mater. **4**, 1824 (2016).
10. I. V. Shadrivov, A. A. Zharov, and Y. S. Kivshar, Appl. Phys. Lett. **83**, 2713 (2003).
11. P. Xiao, J. Opt. Soc. Am. B **28**, 1895 (2011).
12. I. V. Soboleva, V. V. Moskalenko, and A. A. Fedyanin, Phys. Rev. Lett. **108**, 123901 (2012).
13. J. M. Hollas, *Modern Spectroscopy*, 4th ed. (Wiley, 2004).
14. C. W. Hsu, B. Zhen, A. D. Stone, J. D. Joannopoulos, and M. Soljačić, Nat. Rev. Mater. **1**, 16048 (2016).
15. W. Zhang, A. Charous, M. Nagai, D. M. Mittleman, and R. Mendis, Opt. Express **26**, 13195 (2018).
16. S. Fan and J. D. Joannopoulos, Phys. Rev. B **65**, 235112 (2002).
17. S. S. Wang and R. Magnusson, Appl. Opt. **32**, 2606 (1993).
18. S. M. Norton, G. M. Morris, and T. Erdogan, J. Opt. Soc. Am. A **15**, 464 (1998).
19. S. Fan, W. Suh, and J. D. Joannopoulos, J. Opt. Soc. Am. A **20**, 569 (2003).
20. B. Luk'yanchuk, N. I. Zheludev, S. A. Maier, N. J. Halas, P. Nordlander, H. Giessen, and C. T. Chong, Nat. Mater. **9**, 707 (2010).
21. A. E. Miroshnichenko, S. Flach, and Y. S. Kivshar, Rev. Mod. Phys. **82**, 2257 (2010).
22. M. J. Theisen and T. G. Brown, J. Mod. Opt. **62**, 244 (2015).
23. M. F. Limonov, M. V. Rybin, A. N. Poddubny, and Y. S. Kivshar, Nat. Photonics **11**, 543 (2017).
24. J.-P. Connerade and A. M. Lane, Rep. Prog. Phys. **51**, 1439 (1988).
25. H. Lochbihler and R. Depine, Appl. Opt. **32**, 3459 (1993).
26. R. Mendis, M. Nagai, W. Zhang, and D. M. Mittleman, Sci. Rep. **7**, 5909 (2017).
27. P. U. Jepsen, D. G. Cooke, and M. Koch, Laser Photon. Rev. **5**, 124 (2011).